Biochemical and Biophysical Research Communications 441 (2013) 701–706

Contents lists available at ScienceDirect

Biochemical and Biophysical Research Communications

journal homepage: www.elsevier.com/locate/ybbrc

Redox-sensitive structural change in the A-domain of HMGB1 and its implication for the binding to cisplatin modified DNA

Jing Wang [a], Naoya Tochio [b], Aya Takeuchi [a], Jun-ichi Uewaki [a,b], Naohiro Kobayashi [c], Shin-ichi Tate [a,b,*]

[a] Department of Mathematical and Life Sciences, Graduate School of Science, Hiroshima University, Kagamiyama 1-3-1, Higashi-Hiroshima 739-8526, Japan
[b] Research Center for the Mathematics on Chromatin Live Dynamics (RcMcD), Graduate School of Science, Hiroshima University, 1-3-1 Kagamiyama, Higashi-Hiroshima 739-8526, Japan
[c] Protein Research Institute, Osaka University, 3-2 Yamadaoka, Suita 565-0871, Japan

ARTICLE INFO

Article history:
Received 8 October 2013
Available online 25 October 2013

Keywords:
High-mobility group B1
Protein oxidation
NMR structure
Cisplatinated DNA

ABSTRACT

HMGB1 (high-mobility group B1) is a ubiquitously expressed bifunctional protein that acts as a nuclear protein in cells and also as an inflammatory mediator in the extracellular space. HMGB1 changes its functions according to the redox states in both intra- and extra-cellular environments. Two cysteines, Cys23 and Cys45, in the A-domain of HMGB1 form a disulfide bond under oxidative conditions. The A-domain with the disulfide bond shows reduced affinity to cisplatin modified DNA. We have solved the oxidized A-domain structure by NMR. In the structure, Phe38 has a flipped ring orientation from that found in the reduced form; the phenyl ring in the reduced form intercalates into the platinated lesion in DNA. The phenyl ring orientation in the oxidized form is stabilized through intramolecular hydrophobic contacts. The reorientation of the Phe38 ring by the disulfide bond in the A-domain may explain the reduced HMGB1 binding affinity towards cisplatinated DNA.

1. Introduction

Cells use an elaborate mechanism to control protein function in response to oxidative stress through the formation of disulfide bonds between thiol groups [1]. For example, various types of transcription factors exhibit redox-dependent switches that regulate transcriptional activities [2,3]. Recent studies list the proteins regulated by thiol-disulfide exchange [4,5]. Intriguingly, most of the proteins were abundant structural proteins, molecular chaperones and others that are not directly involved in the gene regulation. HMGB1 (high-mobility group B1) is identified as a representative protein with a redox-dependent functional switch [6].

HMGB1 is a ubiquitously expressed nuclear protein, which has two tandem DNA-binding domains, high-mobility group boxes A and B, and a highly acidic C-terminal tail [7]. HMGB1 functions as an architectural chromatin-binding factor that binds to DNA in a structure-specific, yet sequence-independent manner, with higher affinity for unusual DNA structures, including bent, kinked or unwound duplexes [8]. HMGB1 also functions as an extracellular signaling molecule during inflammation, cell differentiation, cell migration and tumor metastasis, and is released from necrotic cells or secreted by activated immune cells [9]. The released HMGB1 oxidizes in the oxidative extracellular space [9–11]. HMGB1 has three cysteine residues. Cys23 and Cys45 in the A-domain are located in close spatial proximity [13], and form a disulfide bond under mild oxidative conditions [11]. The other cysteine, Cys106, in the B-domain is less reactive to oxidative modification; its thiol is buried within the structure [6]. The redox-dependent disulfide bond formation between Cys23 and Cys45 in the A-domain switches the HMGB1 functions in the extracellular space; the HMGB1 in the reduced form functions as a chemoattractant, while the protein with the disulfide bond functions as a proinflammatory cytokine [12].

The redox state of HMGB1 should be functionally relevant also in the intracellular environment, because the redox potential of the A-domain is within the range of the physiological intracellular redox potential [11]. A fraction of HMGB1 should exist in the oxidized form in cells, which could explain the variety of the cellular responses to the HMGB1 engaging gene regulations [13]. The high affinity of HMGB1 to the cisplatinated DNA lesions is expected to enhance the efficacy of cisplatin, a widely used anticancer drugs [14]. HMGB1 binding to the cisplatinated DNA impedes nucleotide excision repair (NER) by shielding the lesions from the repairing proteins [15,16], which thus inhibits replication and transcription in aggressively growing cancer cells, thereby leading to their cell death [17,18]. However, an improvement of the efficacy of cisplatin as a function of HMGB1 protein levels in cells has not been observed [19]. The failure to correlate cell sensitivity to cisplatin with the amount of HMGB1 in cells can be ascribed to

* Corresponding author at: Department of Mathematical and Life Sciences, Graduate School of Science, Hiroshima University, 1-3-1 Kagamiyama, Higashi-Hiroshima 739-8526, Japan.
E-mail address: tate@hiroshima-u.ac.jp (S.-i. Tate).

0006-291X/$ - see front matter © 2013 Elsevier Inc. All rights reserved.
http://dx.doi.org/10.1016/j.bbrc.2013.10.085

the co-existence of the oxidized HMGB1 in cells [13]; the oxidized HMGB1 with the disulfide bond between Cys23 and Cys45 has 10-fold reduced affinity to the cisplatinated DNA, thus reducing the inhibition of the NER process [13]. The oxidization to HMGB1 in cells is, therefore, a factor for the cisplatin resistance of certain tumors [13].

The functional switch according to the redox state of HMGB1 in cells and in the extracellular space has sparked interest to discover new biological roles of this ubiquitously expressed protein. However, the structure of the oxidized A-domain in HMGB1 remains unknown. Therefore, the molecular mechanisms that control functional changes in response to the redox states of HMGB1 remain elusive. To advance our understanding of the redox-dependent functional changes of HMGB1, we have solved the oxidized A-domain structure by NMR. The A-domain in the oxidized form has an unexpectedly large structural change in the loop between helices I and II. In particular, the flipped phenyl ring at Phe38, at the C-terminal edge of the inter-helix loop, relative to that in the structure of the reduced form was remarkable. Phe38 is the key residue interacting into cisplatin-[d(GpG)] intrastrand crosslink sites, as shown in the X-ray complex structure of the reduced A-domain of HMGB1 with the cisplatinated DNA [20]. The significant structural change associated with the disulfide bonding in the A-domain could explain the reduced affinity of the oxidized HMGB1 to the cisplatinated DNA.

2. Materials and methods

2.1. Expression and purification of the oxidized A-domain of HMGB1

HMGB1 A-domain (residues from 1 to 84 of human HMGB1 protein; SwissProt accession IDP09429) was purified from *Escherichia coli*, BL21 (DE3), harboring the corresponding cDNA cloned into pET28a (Merck Chemicals). The purification of the isotopically labeled sample was carried out according to a previously published protocol [21]. His_6-tag at the N-terminus of the HMGB1 A-domain was cleaved by thrombin in 30 units (GE Healthcare) during dialysis against the buffer A solution (50 mM Tris–HCl, pH 8.0) at 4 °C for 16 h. The tag-cleaved A-domain was further purified by Heparin-Sepharose (GE Healthcare) with an NaCl gradient (from 0 to 1 M) in buffer A. Disulfide bond formation in the A-domain was done according to a method published previously [13]; the protein was dialyzed overnight against buffer B (50 mM potassium phosphate with 150 mM KCl, pH 6.4) containing 5 μM $CuCl_2$ at 4 °C and then redialyzed against buffer B without $CuCl_2$. The protein concentration was determined by the OD_{280}. Disulfide bond formation in the final sample was confirmed by electrophoretic mobility in an SDS–PAGE and also by the $^{13}C\beta$ NMR chemical shifts for the Cys23 and Cys 45 residues [22] (Fig. S1).

It is noted that throughout this manuscript, residues in HMGB1 are numbered according to the immature form that retains the initial methionine [23]. The present HMGB1 A-domain fragment has an additional three residues at its N-terminus (i.e., GSH) from the expression vector.

2.2. NMR spectroscopy

A standard set of NMR spectra [24] for resonance assignments of the HMGB1 A-domain in buffer B were collected at 293 K on a Bruker AvanceII spectrometer equipped with a triple resonance cryogenic probe operating at the ^1H resonance frequency of 700 MHz. The ^{15}N–$\{^1H\}$ heteronuclear NOE experiments [24] were performed at 293 K. The experiments for the anisotropic sample using liquid crystals were carried out at 300 K to keep the liquid crystalline media stably aligned. NMR data were processed by NMRPipe [25]. Spectral analyses were done using the KUJIRA suite [26] running on the NMRview [27] platform and SPARKY (T.D. Goddard and Kneller, D.G. SPARKY 3, UCSA). The chemical shift data for the oxidized HMGB1 A-domain have been deposited in the Biological Magnetic Resonance Data Bank (accession code, 11532) (Fig. S2).

2.3. Dipolar coupling measurements

Dipolar couplings ($^1D_{NH}$, $^1D_{C'N}$ and $^2D_{C'H}$) for the $^{13}C/^{15}N$ labeled HMGB1 A-domain in buffer B were simultaneously measured using IPAP-HSQC spectra [28] under selective decoupling to $^{13}C\alpha$ spins. For aligning the protein, a 6% $C_{12}E_5$/hexanol ($r = 0.96$) liquid crystalline medium was used at 300K, which gave a residual deuterium quadrupolar coupling of 8.5 Hz and the magnitudes of the axial alignment tensor component (D_a) and rhombicity (R) were −8.7 Hz and 0.43, respectively.

2.4. Structure determination of the oxidized HMGB1 A-domain

Structure calculations were done with the CYANA program using the automated NOE assignment suite, CANDID [29,30]. The backbone dihedral angle restraints were generated by the TALOS + program [31,32]. The 40 lowest-energy CYANA structures calculated with the distance and the backbone torsion angle restraints were subjected to explicit water refinement with XPLOR-NIH [33,34]. In this refinement, the three types of RDCs ($^1D_{NH}$, $^1D_{C'N}$, and $^2D_{C'H}$) were added to the distance and backbone torsion angle restraints; the RDCs were used by normalizing to the $^1D_{NH}$ data based on the bond lengths and gyromagnetic ratios [35]. The final 20 XPLOR-NIH structures were validated using the program PROCHECK-NMR (Table S1) [36]. The final set of ensemble structure coordinates were deposited in the Protein Data Bank, under the accession code 2RTU.

2.5. Model building of the complex of the oxidized A-domain in HMGB1 with cisplatinated DNA

The complex of the oxidized A-domain in HMGB1 with cisplatinated DNA was modeled on the basis of the X-ray complex structure of cisplatinated DNA and the reduced form of the A-domain (PDB code 1CKT) [20]. The modeling was done as follows. Initially, the minimal essential pairs of the inter-molecular contacting residues were extracted from the coordinates, which enabled us to reproduce the original complex structure using HADDOCK [37]. Subsequently, the same inter-molecular contact residues were used to model the oxidized HMGB1 A-domain with the cisplatinated DNA using HADDOCK [37]. The contacting residues were selected through the analysis of the inter-molecular interactions with the LIGPLOT software [38]; the residues with more than one intermolecular hydrogen bond or more than five non-bonded interactions were chosen. In the complex structure of the cisplatinated DNA with the reduced A-domain, the identified contacting residues were Lys12, Tyr16, Ala17, Arg24, Phe38, Ser42, Lys43, Ser46 and Trp49 in the A-domain and G_8, G_9, A_{10}, C_{11}, C_{12} and T_{13} in one strand, and C_{15}/T_7, C_8 and C_9 in the other strand of the cisplatinated DNA. The docking modeling calculation was done on the HADDOCK web server [39] with the above contacting residues input as the "active" ambiguous interaction residues (AIRs) [37]. For comparison, the same docking calculation was done using the reduced HMGB1 A-domain structure solved under reduced conditions containing 1 mM DTT (PDB code 2YRQ).

3. Results and discussion

3.1. Structural description of the oxidized A-domain of HMGB1

The determined structure of the oxidized A-domain in HMGB1 is shown in comparison with the structure of the reduced form reported previously (PDB code 2YRQ) (Fig. 1A and Fig. S3). The structural statistics are available in Supplementary Material (Table S1). There are notable orientation changes in the N-terminal part of helix II caused by the disulfide bond between Cys23 and Cys45 (Fig. 1A). As shown in the close up view (Fig. 1B), the inter-helix loop between the helices I and II flips over to the concaved surface of the L-shaped structure of the A-domain. The formed disulfide bond shifts the N-terminus of the helix II relative to that observed in the reduced form, and this enables the hydrophobic interaction between the phenyl ring of Phe38 and residues sandwiched by helices I and II (Fig. 1C). This structural observation is supported by the observation that the aromatic protons in Phe38 showed several clear NOEs to the hydrophobic residues inside the concaved surface (Fig. 2), while the corresponding NOEs were not observed in the reduced form A-domain sample.

The intra-molecular contacts of Phe38 with hydrophobic residues limit the flexibility of the inter-helix loop, as evidenced by the changes in the profiles for the ^{15}N–{^{1}H} heteronuclear NOEs (hetNOEs) (Fig. 3). The residues in the inter-helix loop (residues 34–40) showed significantly smaller hetNOE values relative to the secondary structured parts in both reduced and oxidized forms; the corresponding inter-helix loop is more flexible than the other structured parts in the ps–ns time regime [40].

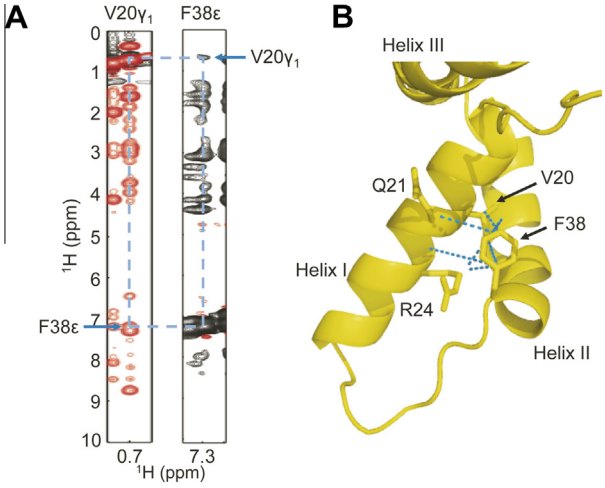

Fig. 2. NOEs to define the flipped ring orientation of Phe38 in the reduced A-domain. (A) The representative strips from the 3D ^{13}C-eddited NOESY data for the reduced A-domain. Val20γ-methyl protons showed clear NOEs to the Phe38 ε ring protons (left panel) and vice versa (right panel). (B) The NOEs derived from the Phe38 ring protons are drawn as blue dotted lines on the structure of the oxidized A-domain; the observed NOEs are listed as V20 Hβ-F38 Hε, V20 Hγ1-F38 Hδ, V20 Hγ1-F38 Hε, V20 Hγ1-F38 Hζ, Q21 Hβ-F38 Hε, R24 HN-F38 Hδ, R24 Hδ-F38 Hδ and R24 Hδ-F38 Hζ. (For interpretation of the references to colour in this figure legend, the reader is referred to the web version of this article.)

Comparison of the hetNOE profiles indicates that residues in the inter-helix loop near Phe38 in the oxidized form showed increased

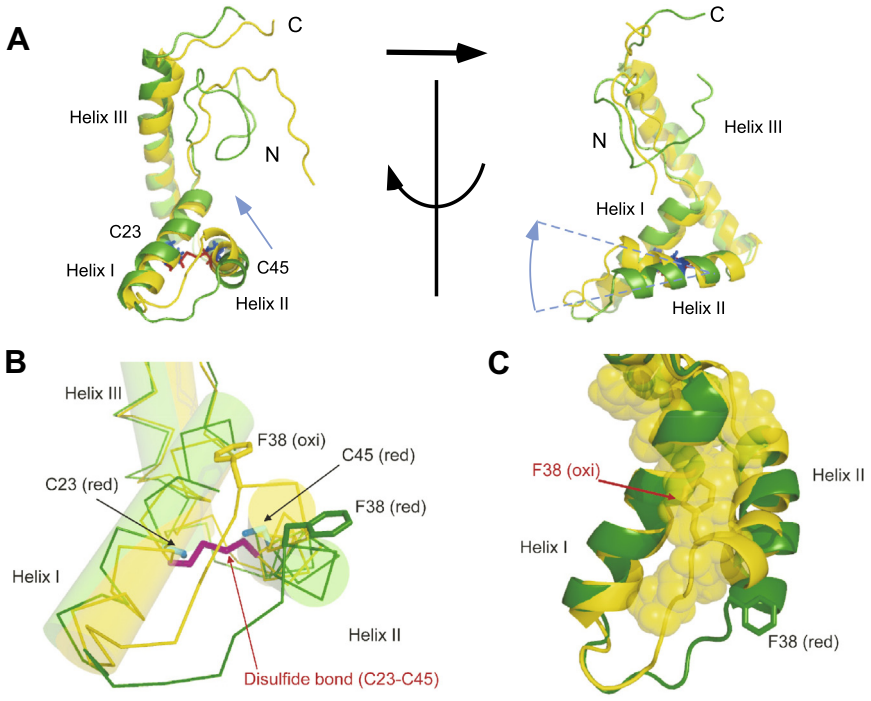

Fig. 1. Structural comparisons of the A-domains in the reduced and oxidized form. (A) Ribbon drawings for the reduced (green; PDB code 2YRQ) and oxidized (yellow) A-domains; two structures were overlaid to minimize the root mean square deviation (rmsd) of the Cα positions in the helices (residues Ser15-Lys30, Phe38-Trp49 and Ala54-Met75). The residues drawn in a ball-and-stick presentation are cysteine residues, Cys23 and Cys45, in the reduced (blue) and oxidized (red) forms. The apparent change in the orientation of the N-terminal part of helix II is emphasized by arrows in blue. The structures on the right are rotated by 90° relative to the structures presented on the left. (B) A close up view of the parts comprising helices I and II with the interhelix linker in the reduced and oxidized A-domain, which demonstrates the flipped Phe38 ring in the oxidized structure (yellow) relative to that in the reduced form. (C) A close up view to show the hydrophobic contacts between the flipped Phe38 in the oxidized A-domain (yellow) with the overlaid reduced form (green). The hydrophobic residues (=F18, F19, F38, F41, F60, V20, V36 and W49) between the helices I and II are drawn as yellow space filling atoms. The figures were prepared by PyMOL (Schrödinger, LLC).

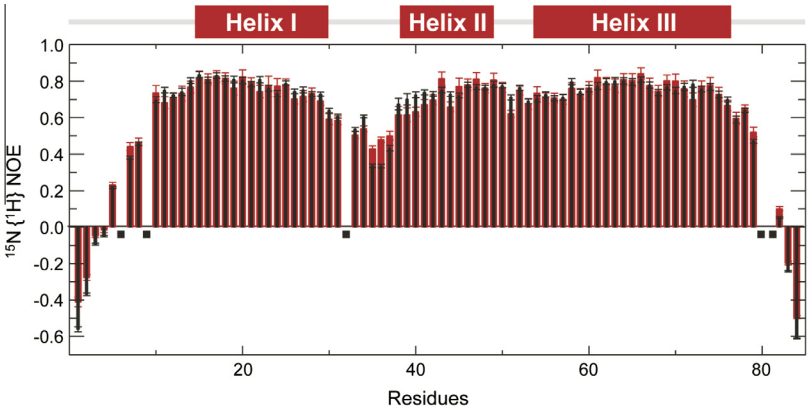

Fig. 3. Comparison of the ^{15}N–{^{1}H} heteronuclear NOEs between the reduced and oxidized A-domains. The values (with errors) for residues in the oxidized and reduced A-domains are plot as red rectangles and black lines, respectively.

hetNOE values; the phenyl ring contact to the hydrophobic residues appears to have reduced the flexibility to the residues.

3.2. Model complex of the oxidized A-domain with the cisplatin-modified DNA

The functional significance of the flipped Phe38 ring in the oxidized form was determined by modeling a complex of the oxidized A-domain with the cisplatinated DNA modeled based on the corresponding X-ray complex structure with the reduced A-domain (PDB code 1CKT) [20].

The HMGB1 A-domain specifically binds to a cisplatin-1,2-intrastrand d(GpG) cross-linked (cisplatin-[d(GpG)]) DNA [14]. The crystal structure demonstrated that the increased affinity of the A-domain for the cisplatinated DNA is mediated by an intercalation of the phenyl ring of Ph38 into the platinated lesion (Fig. 4) [20]. The phenyl ring is inserted into a hydrophobic cavity formed by the platinum-modified neighboring guanine rings [20]. The stacking interactions between the phenyl ring and its surrounding guanine bases may stabilize the overall protein-DNA complex. The HMGB1 A-domain has limited affinity to the canonical double-stranded DNA, while the B-domain has higher affinity to such a double-stranded DNA structure [41]. The enhanced affinity of the A-domain to the cisplatinated DNA by the phenyl ring intercalation determines the specific binding of the full-length HMGB1 to the cisplatinated DNA.

The reduced A-domain structure solved in a DNA free-state (PDB code 2YRQ) was docked onto the cisplatinated DNA using the HADDOCK program [37]. The phenyl ring of Phe38 in the docked structure is close to that found in the X-ray structure (Fig. 4). The phenyl ring in the reduced A-domain could intercalate with the platinated guanine bases by a subtle ring reorientation (Fig. 4B). The model complex structure, therefore, satisfactorily explains the high affinity of the reduced A-domain towards the cisplatinated DNA.

The Phe38 ring moiety in the oxidized A-domain with the flipped orientation against that in the reduced form is not allowed for intercalating into the cisplatin-[(GpG)] lesion in the model complex (Fig. 4B).

3.3. Structural explanation for the reduced binding of the oxidized A-domain to the cisplatinated DNA

As discussed above, the intercalation of the phenyl ring of Phe38 into the palatinate guanine bases is the key interaction that enhances the HMGB1 binding to the cisplatinated DNA. As seen in

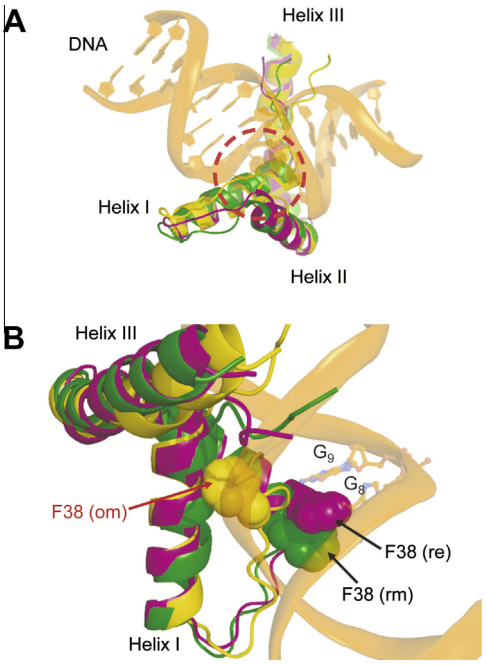

Fig. 4. Comparing the model complexes with the crystal structure of the reduced A-domain with cisplatinated DNA. (A) The modeled complex structures with the A-domains in the reduced (PDB code 2YRQ) and the oxidized forms solved in the DNA-free state are superimposed onto the X-ray complex structure (PDB code 1CKT). The cisplatin-[d(GpG)] part is marked with a red dotted circle. The A-domain structures are drawn in ribbon representations; the reduced A-domain in the X-ray complex (magenta; re), the reduced (green; rm) and oxidized (yellow; om) A-domains in the model structures. The displatinated DNA is drawn in pink ribbon. (B) Close up views around the platinated site to compare the interactions of the Phe38 ring moiety to the cavity made by the cisplatinated-[d(GpG)]. Structures are drawn with the same color usage as in (A), with space-filling representation to the phenyl rings at Phe38. The figures were prepared by the program UCSF Chimera [42].

the model complex with the reduced A-domain structure solved in the DNA free-state, the slight reorientation of the phenyl ring achieves a stable interaction between the A-domain and the cisplatinated DNA (Fig. 4B). Conversely, the model complex using the oxidized A-domain has demonstrated that the phenyl ring could not readily intercalate into the cavity by the platinated guanine bases (Fig. 4B). The phenyl ring stably remains within the hydrophobic core in the oxidized A-domain (Fig. 1C). Such interactions are sufficiently stable to give a significant number of NOEs among

the residues (Fig. 2). In addition, this phenyl ring mediated interaction limits the structural flexibility of the inter-helix loop as shown by the hetNOE profiles (Fig. 3). Taking these spectroscopic results together, the phenyl ring could retain the flipped orientation in the complex with the cisplatinated DNA, but cannot intercalate into the platinated lesion as shown in the model complex structure (Fig. 4B). In addition, the phenyl ring in the oxidized A-domain directs towards the opposite side from the platinated guanine bases in the complex, in which the phenyl ring reorientation to intercalate with the DNA may not be induced (Fig. 4B). These structure-based observations explain the reduced affinity of the A-domain of HMGB1 toward the cisplatin modified DNA.

In summary, this study has shown the significant structural difference in the oxidized A-domain of HMGB1 from that of the structure of the reduced form. In the oxidized A-domain structure the phenyl ring of Phe38 faces onto the concaved surface of the L-shaped structure, whereas the ring in the reduced form extrudes to function as a wedge intercalating into the platinated lesion in the DNA. As experimentally shown, the withdrawn form of the phenyl ring would be sufficiently stable to maintain the structure even in the complex with the cisplatinated DNA. The phenyl ring in the oxidized form, therefore, cannot wedge into the cisplatinated DNA; however, other interactions observed with the DNA are similar to those seen in the reduced A-domain-DNA complex. The flipping of the phenyl ring caused by the disulfide bond may represent the primary reason for the one-order lower binding affinity of the oxidized A-domain when compared with the binding affinity of the reduced form protein [13].

Acknowledgments

We thank Dr. Sachiko Machida at the National Agriculture and Food Research Organization for providing us with the human HMGB1 cDNA. This work was supported by a Grant-in-Aid for Scientific Research on Innovative Areas: "Molecular Science on Fluctuation toward Biological Functions" from the JSPS.

Appendix A. Supplementary data

Supplementary data associated with this article can be found, in the online version, at http://dx.doi.org/10.1016/j.bbrc.2013.10.085.

References

[1] H.E. Marshall, K. Merchant, J.S. Stamler, Nitrosation and oxidation in the regulation of gene expression, FASEB J. 14 (2000) 1889–1900.
[2] A.-P. Arrigo, Gene expression and the thiol redox state, Free Radical Biol. Med. 27 (1999) 936–944.
[3] S.O. Kim, K. Merchant, R. Nudelman, W.F. Beyer, T. Keng, J. DeAngelo, A. Hausladen, J.S. Stamler, OxyR: a molecular code for redox-related signaling, Cell 109 (2002) 383–396.
[4] H. Yano, J.H. Wong, Y.M. Lee, M.-J. Cho, B.B. Buchanan, A strategy for the identification of proteins targeted by thioredoxin, Proc. Nat. Acad. Sci. 98 (2001) 4794–4799.
[5] C. Lind, R. Gerdes, Y. Hamnell, I. Schuppe-Koistinen, H.B. von Löwenhielm, A. Holmgren, I.A. Cotgreave, Identification of S-glutathionylated cellular proteins during oxidative stress and constitutive metabolism by affinity purification and proteomic analysis, Arch. Biochem. Biophys. 406 (2002) 229–240.
[6] G. Hoppe, K.E. Talcott, S.K. Bhattacharya, J.W. Crabb, J.E. Sears, Molecular basis for the redox control of nuclear transport of the structural chromatin protein Hmgb1, Exp. Cell Res. 312 (2006) 3526–3538.
[7] J.O. Thomas, A.A. Travers, HMG1 and 2, and related 'architectural' DNA-binding proteins, Trends Biochem. Sci. 26 (2001) 167–174.
[8] J.O. Thomas, HMG1 and 2: architectural DNA-binding proteins, Biochem. Soc. Trans. 29 (2001) 395–401.
[9] D. Tang, R. Kang, H.J. Zeh 3rd, M.T. Lotze, High-mobility group box 1, oxidative stress, and disease, Antioxid. Redox Signal. 14 (2011) 1315–1335.
[10] L. Zandarashvili, D. Sahu, K. Lee, Y.S. Lee, P. Singh, K. Rajarathnam, J. Iwahara, Real-time kinetics of high-mobility group box 1 (HMGB1) oxidation in extracellular fluids studied by in situ protein NMR spectroscopy, J. Biol. Chem. 288 (2013) 11621–11627.
[11] D. Sahu, P. Debnath, Y. Takayama, J. Iwahara, Redox properties of the A-domain of the HMGB1 protein, FEBS Lett. 582 (2008) 3973–3978.
[12] E. Venereau, M. Casalgrandi, M. Schiraldi, D.J. Antoine, A. Cattaneo, F. De Marchis, J. Liu, A. Antonelli, A. Preti, L. Raeli, S.S. Shams, H. Yang, L. Varani, U. Andersson, K.J. Tracey, A. Bachi, M. Uguccioni, M.E. Bianchi, Mutually exclusive redox forms of HMGB1 promote cell recruitment or proinflammatory cytokine release, J. Exp. Med. 209 (2012) 1519–1528.
[13] S. Park, S.J. Lippard, Redox state-dependent interaction of HMGB1 and cisplatin-modified DNA, Biochemistry 50 (2011) 2567–2574.
[14] P.M. Pil, S.J. Lippard, Specific binding of chromosomal protein HMG1 to DNA damaged by the anticancer drug cisplatin, Science 256 (1992) 234–237.
[15] I. Ugrinova, S. Zlateva, I.G. Pashev, E.A. Pasheva, Native HMGB1 protein inhibits repair of cisplatin-damaged nucleosomes in vitro, Int. J. Biochem. Cell Biol. 41 (2009) 1556–1562.
[16] J.C. Huang, D.B. Zamble, J.T. Reardon, S.J. Lippard, A. Sancar, HMG-domain proteins specifically inhibit the repair of the major DNA adduct of the anticancer drug cisplatin by human excision nuclease, Proc. Natl. Acad. Sci. USA 91 (1994) 10394–10398.
[17] J.A. Mello, S.J. Lippard, J.M. Essigmann, DNA adducts of cis-diamminedichloroplatinum(II) and its trans isomer inhibit RNA polymerase II differentially in vivo, Biochemistry 34 (1995) 14783–14791.
[18] M. Shimizu, B. Rosenberg, A similar action to UV-irradiation and a preferential inhibition of DNA synthesis in E. coli by antitumor platinum compounds, J. Antibiotics 26 (1973) 243–245.
[19] M. Wei, O. Burenkova, S.J. Lippard, Cisplatin sensitivity in Hmbg1-/- and Hmbg1+/+ mouse cells, J. Biol. Chem. 278 (2003) 1769–1773.
[20] U.M. Ohndorf, M.A. Rould, Q. He, C.O. Pabo, S.J. Lippard, Basis for recognition of cisplatin-modified DNA by high-mobility-group proteins, Nature 399 (1999) 708–712.
[21] J.-i. Uewaki, H. Kamikubo, J.-i. Kurita, N. Hiroguchi, H. Moriuchi, M. Yoshida, M. Kataoka, N. Utsunomiya-Tate, S.-i. Tate, Preferential domain orientation of HMGB2 determined by the weak intramolecular interactions mediated by the interdomain linker, Chem. Phys. 419 (2013) 212–223.
[22] D. Sharma, K. Rajarathnam, 13C NMR chemical shifts can predict disulfide bond formation, J. Biomol. NMR 18 (2000) 165–171.
[23] R. Sterner, G. Vidali, V.G. Allfrey, Studies of acetylation and deacetylation in high mobility group proteins. Identification of the sites of acetylation in HMG-1, J. Biol. Chem. 254 (1979) 11577–11583.
[24] J. Cavanagh, W.J. Fairbrother, A.G. Palmer III, N.J. Skelton, Heteronuclear NMR Experiments, Academic Press Inc., New York, 1996.
[25] F. Delaglio, S. Grzesiek, G.W. Vuister, G. Zhu, J. Pfeifer, A. Bax, NMRPipe: a multidimensional spectral processing system based on UNIX pipes, J. Biomol. NMR 6 (1995) 277–293.
[26] N. Kobayashi, J. Iwahara, S. Koshiba, T. Tomizawa, N. Tochio, P. Güntert, T. Kigawa, S. Yokoyama, KUJIRA, a package of integrated modules for systematic and interactive analysis of NMR data directed to high-throughput NMR structure studies, J. Biomol. NMR 39 (2007) 31–52.
[27] B. Johnson, Using NMRView to visualize and analyze the NMR spectra of macromolecules, in: A.K. Downing (Ed.), Protein NMR Techniques, vol. 278, Humana Press, 2004, pp. 313–352.
[28] M. Ottiger, F. Delaglio, A. Bax, Measurement of J and dipolar couplings from simplified two-dimensional NMR spectra, J. Magn. Reson. 131 (1998) 373–378 (San Diego, Calif.: 1997).
[29] P. Güntert, Automated NMR Structure Calculation With CYANA, in: A.K. Downing (Ed.), Protein NMR Techniques, 278, Humana Press, 2004, pp. 353–378.
[30] T. Herrmann, P. Güntert, K. Wüthrich, Protein NMR structure determination with automated NOE assignment using the new software CANDID and the torsion angle dynamics algorithm dyana, J. Mol. Biol. 319 (2002) 209–227.
[31] Y. Shen, F. Delaglio, G. Cornilescu, A. Bax, TALOS+: a hybrid method for predicting protein backbone torsion angles from NMR chemical shifts, J. Biomol. NMR 44 (2009) 213–223.
[32] G. Cornilescu, F. Delaglio, A. Bax, Protein backbone angle restraints from searching a database for chemical shift and sequence homology, J. Biomol. NMR 13 (1999) 289–302.
[33] J.P. Linge, M.A. Williams, C.A.E.M. Spronk, A.M.J.J. Bonvin, M. Nilges, Refinement of protein structures in explicit solvent, Proteins: Structure, Function, and Bioinformatics 50 (2003) 496–506.
[34] C.D. Schwieters, J.J. Kuszewski, N. Tjandra, G. Marius Clore, The Xplor-NIH NMR molecular structure determination package, J. Magn. Reson. 160 (2003) 65–73.
[35] A. Bax, G. Kontaxis, N. Tjandra, Dipolar couplings in macromolecular structure determination, in: V.D. Thomas, L. James, S. Uli (Eds.), Methods in Enzymology, vol. 339, Academic Press, 2001, pp. 127–174.
[36] R.A. Laskowski, J.A. Rullmannn, M.W. MacArthur, R. Kaptein, J.M. Thornton, AQUA and PROCHECK-NMR: programs for checking the quality of protein structures solved by NMR, J. Biomol. NMR 8 (1996) 477–486.
[37] C. Dominguez, R. Boelens, A.M. Bonvin, HADDOCK: a protein-protein docking approach based on biochemical or biophysical information, J. Am. Chem. Soc. 125 (2003) 1731–1737.
[38] A.C. Wallace, R.A. Laskowski, J.M. Thornton, LIGPLOT: a program to generate schematic diagrams of protein–ligand interactions, Protein Eng. 8 (1995) 127–134.
[39] S.J. de Vries, M. van Dijk, A.M. Bonvin, The HADDOCK web server for data-driven biomolecular docking, Nat. Protoc. 5 (2010) 883–897.

[40] A.G. Palmer Iii, Probing molecular motion by NMR, Curr. Opin. Struct. Biol. 7 (1997) 732–737.
[41] A. Travers, Recognition of distorted DNA structures by HMG domains, Curr. Opin. Struct. Biol. 10 (2000) 102–109.
[42] E.F. Pettersen, T.D. Goddard, C.C. Huang, G.S. Couch, D.M. Greenblatt, E.C. Meng, T.E. Ferrin, UCSF Chimera—A visualization system for exploratory research and analysis, J. Comput. Chem. 25 (2004) 1605–1612.